nature communications

Article

https://doi.org/10.1038/s41467-025-60219-0

Frustrated phonon with charge density wave in vanadium Kagome metal

Received: 26 March 2025

Accepted: 16 May 2025

Published online: 26 May 2025

Check for updates

Seung-Phil Heo[1,2,3], Choongjae Won[4], Heemin Lee[1,2,3], Hanbyul Kim[5], Eunyoung Park[1,2,3], Sung Yun Lee[1,2,3], Junha Hwang[1,2,3], Hyeongi Choi[6], Sang-Youn Park[6], Byungjune Lee[1,3,4], Woo-Suk Noh[4,6], Hoyoung Jang[3,6], Jae-Hoon Park[1,3,4], Dongbin Shin[5,7] ✉ & Changyong Song[1,2,3] ✉

The formation of a star-of-David charge density wave superstructure, resulting from the coordinated displacements of vanadium ions on a corner-sharing triangular lattice, has garnered significant attention to comprehend the influence of electron–phonon interaction within geometrically intricate lattice of Kagome metals, specifically AV_3Sb_5 (where A represents K, Rb, or Cs). However, understanding of the underlying mechanism behind charge density wave formation, coupled with symmetry-protected lattice vibrations, remains elusive. Here, from femtosecond time-resolved X-ray scattering experiments, we reveal that the phonon mode, associated with cesium ions' out-of-plane motion, becomes frustrated in the charge density wave phase. Furthermore, we observed the photoinduced emergence of a metastable charge density wave phase, facilitated by alleviating the frustration. By not only elucidating the longstanding puzzle surrounding the intervention of phonons but introducing the phononic frustration, this research offers insights into the competition between phonons and periodic lattice distortions, a phenomenon widespread in other correlated quantum materials including layered high-temperature superconductors.

Crystals with unique ionic arrangements and strong electronic correlations serve as a fertile ground for the emergence of exotic phases, as evidenced by the coexistence of charge density wave (CDW) and superconductivity in vanadium (V) Kagome metals of AV_3Sb_5 (A for K, Rb, and Cs). Exotic phases involving CDW and superconductivity (SC), arising from intricate electronic structures within geometrically frustrated ionic arrangements, have spurred active investigation into the Kagome metal, AV_3Sb_5 (Fig. 1a)[1,2]. Experimental findings suggest that mechanisms driving CDW formation extend beyond Peierls distortion that is facilitated by enhanced electron–phonon interactions through nested Fermi surfaces. This has led to new hypotheses regarding electron–hole pairing mediated by phonons[3–6]. The van Hove singularity of V *d*-electrons near the Fermi level has been proposed as a pivotal factor in CDW instability[7,8]. However, the role of phonons remains ambiguous, as phonon softening, a characteristic of CDW instability, has not been observed to the best of our knowledge[5,9]. Additionally, the CDW and SC phases exhibit sensitivity to different choices of alkali metal ions in the Kagome system[10–14], despite the limited presence of electron population from the cations near the Fermi level[7,8]. These findings suggest that the electronic potential energy surface may undergo dramatic changes due to cation movement, giving rise to such diverse phases. While there have been several

[1]Department of Physics, POSTECH, Pohang, Korea. [2]Center for Ultrafast Science on Quantum Matter, Max Planck POSTECH/Korea Research Initiative, Pohang, Korea. [3]Photon Science Center, POSTECH 37673, Pohang, Korea. [4]Center for Complex Phase Materials, Max Planck POSTECH/Korea Research Initiative, Pohang, Korea. [5]Department of Physics and Photon Science, Gwangju Institute of Science and Technology, Gwangju, Korea. [6]Pohang Accelerator Laboratory, POSTECH, Pohang, Korea. [7]Max Planck Institute for the Structure and Dynamics of Matter, Hamburg, Germany. ✉e-mail: dshin@gist.ac.kr; cysong@postech.ac.kr

https://doi.org/10.1038/s41467-025-60219-0

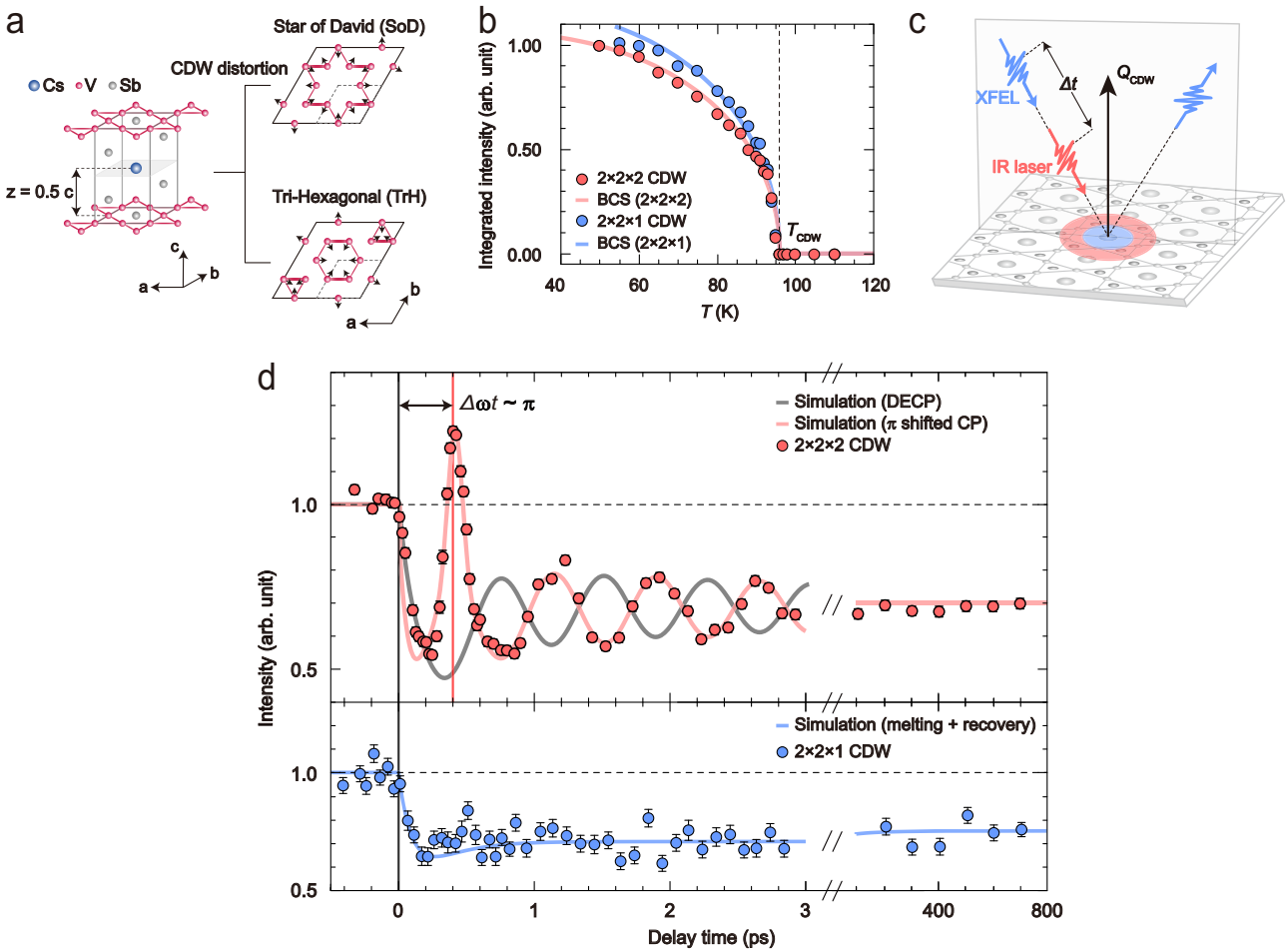

Fig. 1 | Time-resolved X-ray scattering investigation of CDW superstructures of CsV_3Sb_5. **a** Crystal structure of CsV_3Sb_5 with the vanadium-networked Kagome lattice. **b** CDW order parameters derived from the integrated intensities of the (0.5 0 2) and (0.5 0 1.5) reflections representing the $2\times2\times1$ and $2\times2\times2$ superstructures, respectively. Solid lines depict results from BCS gap equations. **c** Schematic representation of time-resolved X-ray scattering experiments. **d** Temporal evolution of the $2\times2\times1$ and $2\times2\times2$ CDW reflections showing photoinduced melting and recovery. Ultrafast melting within 100 fs is commonly observed for both $2\times2\times1$ and $2\times2\times2$, with the peak intensity not fully recovering immediately. Solids lines are from simulations (text). Error bars indicate the standard error of the peak intensity. Notably, intensity oscillation is observed for the $2\times2\times2$ CDW. It results from a coherent phonon oscillation (red line) but with a phase delay of ωt ~ 400 fs, distinguished from normal displacement excited coherent phonon (DECP, grey line).

ultrafast optical and ARPES studies on CDW phases[15–17], further research into the microscopic CDW orderings in excited states remains necessary.

In this work, we conducted femtosecond (fs) time-resolved X-ray scattering experiments on CsV_3Sb_5 to investigate CDW instabilities within a finely balanced potential energy landscape, induced by photoexciting electrons near the Fermi level of the range of ~ 1.5 eV matching with the photon energy of fs-infrared (IR) laser pulses. Mostly electrons in V and Sb ions' orbitals are involved in this photoexcitation process[5,18]. Notably, we find that the phonon mode involving Cs ions' out-of-plane motion becomes energetically frustrated in the CDW phase, impeding its immediate participation in CDW formation. Furthermore, our study reveals that femtosecond laser excitation alleviates this frustration, triggering an asymmetric phonon response and enabling the emergence of a metastable CDW state. X-ray scattering experiments were conducted utilising the Pohang Accelerator Laboratory X-ray Free Electron Laser (PAL-XFEL) and the Pohang Light Source (PLS).

Results

The emergence of superstructures below the CDW transition temperature of 96 K was confirmed, revealing the coexistent $2\times2\times1$ and $2\times2\times2$ CDWs (notated as $a\times b\times c$ in multiples of the unit cell) (Fig. 1a, b)[19]. Doubling of the unit cell in the *ab*-plane resulted in a 2×2 superstructure due to in-plane displacements of V ions, forming a star-of-David (SoD) or its inverse triangle-and-hexagon (TrH) pattern (Fig. 1a)[10,20,21]. Additionally, unit cell doubling along the *c*-axis was observed, establishing the $2\times2\times2$ superstructure. Another lattice instability is required to induce this superstructure with the phonon mode (L_2^-) involving ions' *c*-directional motion attributed to driving this instability[9,15]. The $2\times2\times1$ and $2\times2\times2$ CDWs, corresponding to in-plane distortion with in-phase and phase shifted stacking along the *c*-direction[20], respectively, were identified with different peak widths and temperature dependence of intensities at $Q_{CDW}^{2\times2\times1}=(0.50\text{Integer})$ and $Q_{CDW}^{2\times2\times2}=(0.50\text{Integer}+0.5)$. They present in the same physical domain as same CDWs but with a variation in a *c*-directional stacking. The order parameters are derived from the integrated intensities of the CDW satellites (Fig. 1b and Supplementary Note 1)[5,6,22].

The rapid redistribution of electrons near the Fermi level due to fs-IR photoexcitation disturbed these CDW orderings. Subsequently, the ultrafast reaction dynamics of the CDWs were investigated using femtosecond X-ray pulses from the PAL-XFEL (Fig. 1c and Method). The temporal evolution of peak intensity from the $2\times2\times2$ CDW reflection exhibited an oscillation without full recovery until approximately 2 ns, whereas no oscillation was observed for the $2\times2\times1$ CDW (Fig. 1d). These features were explicitly resolved by simulating exponential

https://doi.org/10.1038/s41467-025-60219-0

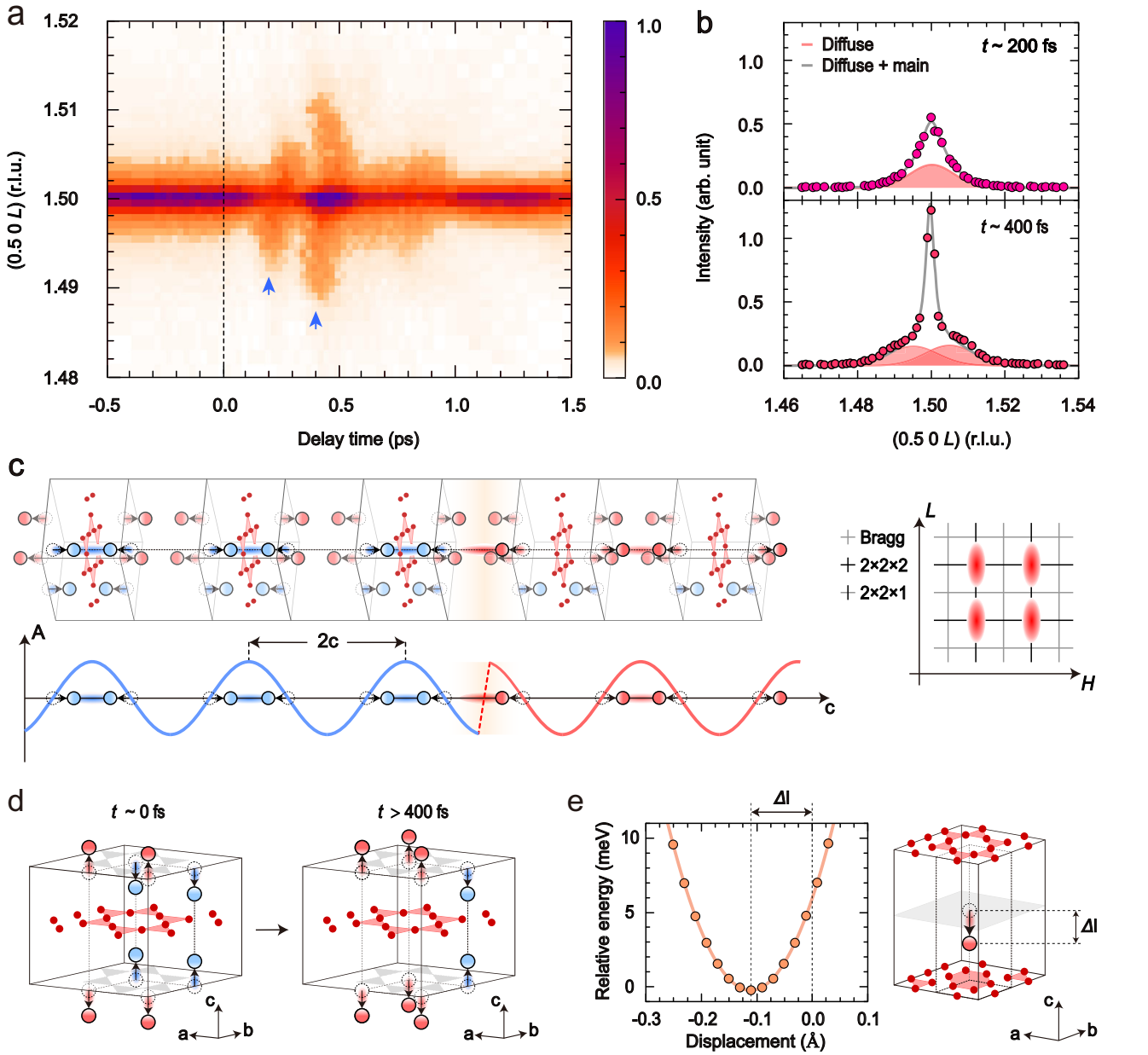

Fig. 2 | Metastable CDW states with localised phonon mode. a Photoinduced melting of the 2 × 2 × 2 CDW with strong diffuse signals developed along the *c*-direction at ~ 200 fs and 400 fs (blue arrows). The color scale represents the normalized intensity. **b** The *L*-scan at 400 fs displays diffusive two-wing structure, centered on 2 × 2 × 2 CDW reflection, caused by a phase slip in the CDW domain (lower panel), distinguishable from the signal at 200 fs with diffuse tails resulting from reduced domain size (upper panel). **c** Phase-slip in the 2×2 × 2 CDW. The red-coloured sinusoidal wave indicates the domain with three-one Cs displacements newly formed from the native two-two vibration (blue colour). The orange area and dotted red line denote a CDW phase-slipped region. Right panel displays the diffuse scattering pattern corresponding to this phase-slip structure. **d** Comparison between the symmetric but energetically frustrated two-two vibration in the native CDW and the modified, frustration-relieved Cs vibration initiated at ~ 400 fs, which persists as a metastable CDW ordering. In panels (**c**, **d**), the red and blue shaded circles represent Cs ions, the red line with red circles illustrates the vanadium kagome net, and the grey lines indicate the 2 × 2 × 2 unit cell. **e** Potential energy surface calculation with an eye-guide solid line demonstrates that Cs ions, located at the centre of the 2 × 2 dimerised V structure, become more stable by moving toward (or out of) the TrH (SoD) mesh.

decay and recovery reactions (drawn with a solid line) (Supplementary Note 2). Both CDWs underwent rapid melting at approximately 100 fs, followed by a quick yet partial recovery of intensity in 300 fs. These timescales match with previously reported in CDW systems with electron–phonon interactions[17,23,24]. After the photoinduced melting, rapid reconstruction of the CDW within hundreds of femtoseconds was observed, but into a metastable state with reduced intensity involving an asymmetric vibration of Cs ions changed from the intact CDW's native L_2^- mode. This metastable state, persisting for nanoseconds, is induced by photoinduced electronic perturbation rather than thermal disorder as noted by slow recovery of Bragg reflection in several hundred picoseconds (Supplementary Note 3)[25].

The oscillating intensity of the 2 × 2 × 2 CDW reflected a coherent phonon with a frequency of approximately 1.3 THz. This resembles aforementioned L_2^- phonon but with a critical difference[9,15]. One should note that native L_2^- phonon involves symmetric motions of two Cs ions moving upward while the other two move downward, exhibiting a specific symmetry. From the 3*Q* degenerate CDW structure of

https://doi.org/10.1038/s41467-025-60219-0

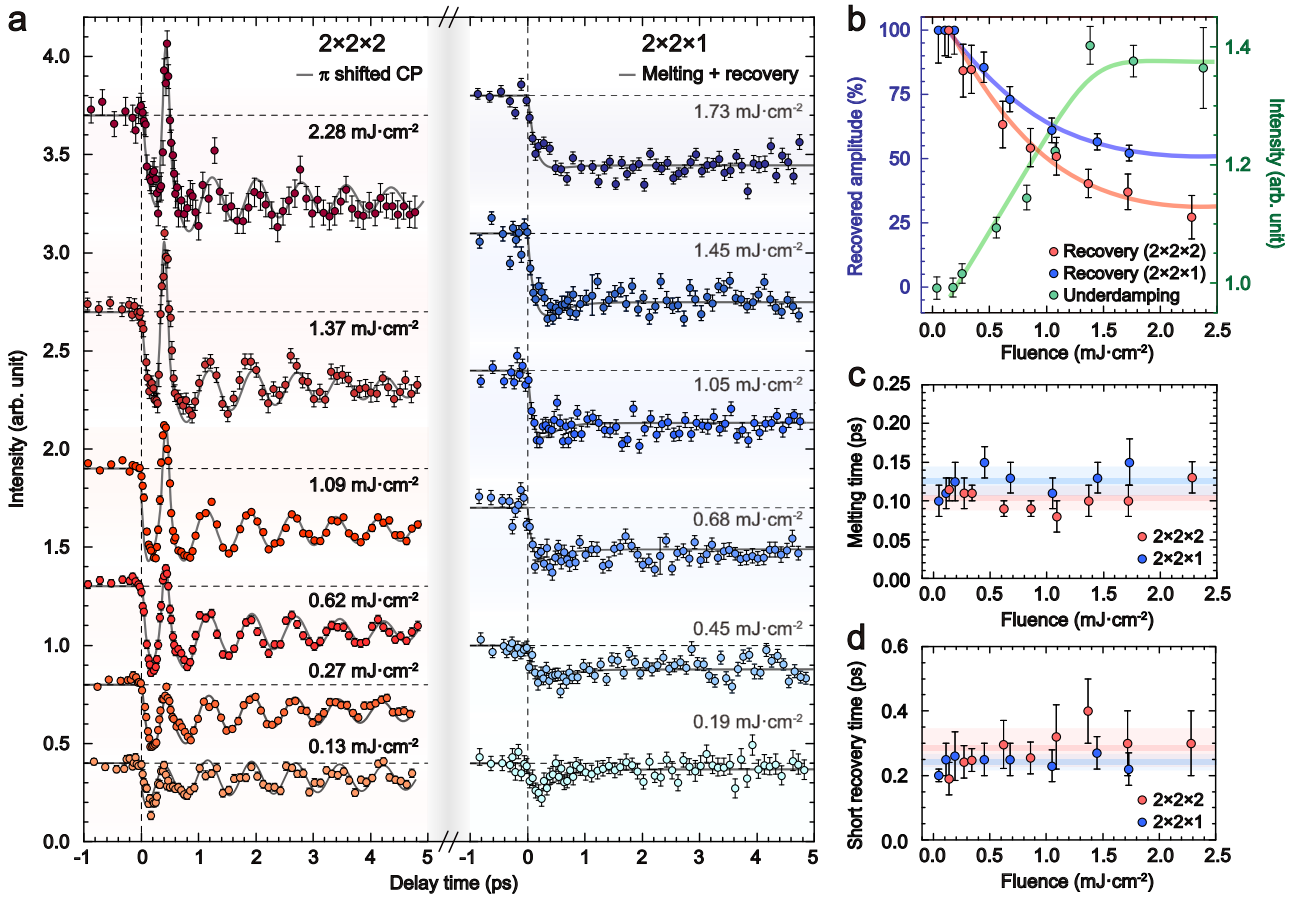

Fig. 3 | Laser fluence dependence of CDW melting and recovery. a Laser fluence dependence of the 2 × 2 × 2 (left) and 2 × 2 × 1 CDW (right) peak intensities, showing a larger reduction in peak intensities with higher laser fluence. Underdamped intensity at ~ 400 fs develops more strongly in the 2 × 2 × 2 CDW with increasing laser fluence, but the oscillation period is insensitive to the laser fluence. The horizontal dashed lines indicate a peak intensity value of 1, representing the idealized baseline intensity before time zero. Error bars indicate the standard error of the peak intensity. **b** Intensities of partially recovered CDWs obtained for different laser fluences, showing a similar behaviour of gradual decrease until ~ 1.4 mJ cm^{-2} before saturation. Intensity of the underdamped oscillation at 400 fs is also compared, displaying a similar pattern of monotonic increase until 1.4 mJ cm^{-2} followed by saturation (right). **c**, **d** Comparison of melting and short recovery time of the two CDWs, displaying a similar timescale for melting in 100 fs and short recovery in ~ 300 fs without notable dependence on laser fluence. Solid lines, in (**b**–**d**, are guide to eyes. Error bars in b to d represent the fitting error obtained from simulation functions (Supplementary Note 2).

this system, this phonon mode can affect the 2 × 2 × 2 superstructure intensity but only for the one case out of three CDWs, as a minor contribution. (Supplementary Note 4)[15,20]. Hence, the observed oscillatory intensity suggests a fundamental modification of the native L_2^- phonon, which induces intensity variations across all triply degenerate CDW states, caused by the fs-IR photoexcitation of conduction electrons. Consistent with this, the coherent phonons detected through CDW reflection exhibited an unusual phase delay of approximately π (Supplementary Note 2)[26,27]. This phase delay indicates the presence of competing interactions that delay the prompt excitation of coherent phonons and distort the native phonon mode[28–30].

The emergence of strong diffuse signals along the *c*-direction around the 2 × 2 × 2 CDW reflection strongly supports the interpretation of competing interactions between the 2 × 2 × 2 CDW and the L_2^- phonon mode (Fig. 2a). The first diffuse streak, which developed at 200 fs, was of the ordinary type resulting from CDW melting, with a reduced domain size of approximately 60% of the intact value (Fig. 2b). As the peak sharpened with CDW reconstruction, another strong diffuse streak appeared at around 400 fs, coinciding with the delayed onset of the coherent phonon (Fig. 2b). This transiently formed diffuse signal, observed at approximately 400 fs, exhibited a two-wing structure relative to the main CDW reflection. These diffuse scattering peaks developed at positions with symmetric offsets ($\pm \delta q \sim 5 \times 10^{-3}\ 2\pi/c$) relative to the 2 × 2 × 2 CDW superstructure at 1.5 ($2\pi/c$), arising from disordered phase slip while relieving the frustrated phonon (Fig. 2b)[31–33]. The two-wing structure represents random period in the phase slip (Supplementary Note 5).

Other possibilities on the origin of the diffuse peaks have been attempted to include thermal diffuse scattering[34], order-disorder transitions[35], or critical scattering. Observed broad diffuse tail extending to inelastic excitation up to ~3 eV, and with symmetric contribution, is beyond ordinary quasiparticle excitations. The order-disorder transitions often involving in single broad diffuse scattering is not the current case. A possibility of critical scattering with two lengths scale, ordered region with long correlation along with disordered domains short correlation length, can be considered, which usually happen near the phase transition point[36]. We do not explicitly rule out this possibility but want to mention that such two length scale peaks were not observed in static temperature dependent measurement, not to support such interpretation. Yet, our phase-slip domain interpretation generally accounts for the observed intensity pattern.

Here, we present a schematic model describing the phase slip resulted from the asymmetric alterations: three-up (down) and one-down (up) deviated from the symmetric two-up and two-down displacements (Fig. 2c). The proposed structural model was consistent with the diffuse scattering pattern developed along the *c*-direction (Supplementary Note 5). One notes that increased disorder in phase slip domain size results in broadened width of the satellite diffuse

https://doi.org/10.1038/s41467-025-60219-0

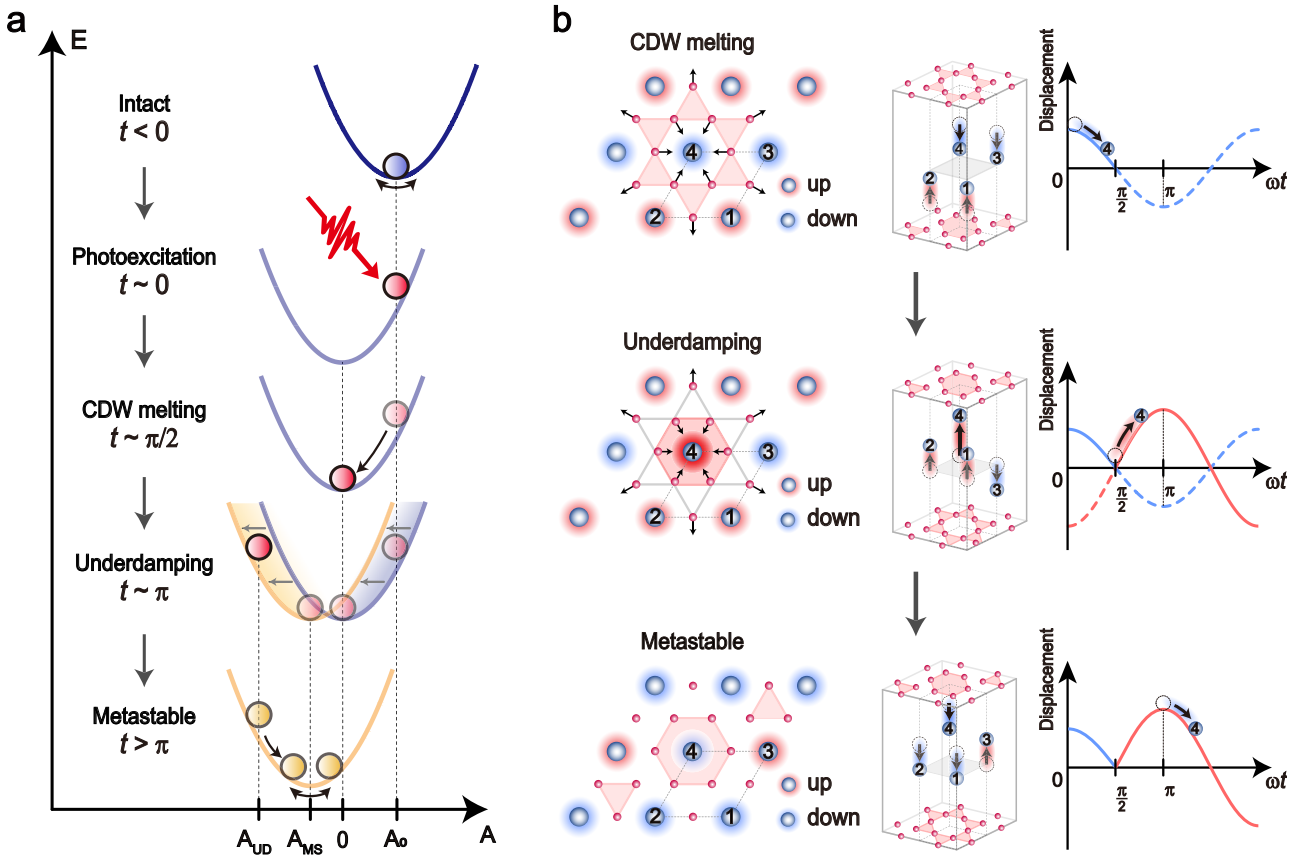

Fig. 4 | Photoinduced underdamping and metastable state of 2 × 2 × 2 CDW. **a** Ultrafast reaction in the 2 × 2 × 2 CDW depicted by a pictorial view of photo-induced potential energy changes with the CDW amplitude (A). Fs-IR pumping shifts the potential energy to the ground state without CDW (A = 0) caused by photoinduced gap closing (t ~ 0). Following this transiently formed potential energy, the CDW melts to reach the energy ground state (ωt ~ π /2). While adapting to this new potential, underdamped displacement of the CDW occurs (ωt ~ π) with further displacement of the potential energy surface having the ground state at A_{MS}. The CDW amplitude now oscillates around the new ground state amplitude, A_{MS}, of the metastable state. **b** Fs-IR pumping alters Cs ions' c-directional vibration (L_2^- phonon) in a manner to relieve energetically frustrated two-two displacements. Blue circles represent Cs ions, while red circles outlined with grey lines form the vanadium kagome network. The red shaded region indicates the vanadium CDW formation. Upon abrupt disturbance of the electron distribution by fs-IR pumping, the frustrated symmetric (two-up and two-down) phonon mode changes to three-one, compatible with the total energy. The right panel shows the path of the symmetric phonon mode (blue sinusoidal line) changing into the path of the asymmetric phonon mode (red sinusoidal line).

peaks to bury the two-peak structure to a single diffusive peak alongside a sharp CDW reflection (Supplementary Note 5). However, this also reflects on a phase slip consistent with the present interpretation.

Further to confirm the modification of the native L_2^- phonon mode after the photoexcitation, we have carried out time-dependent density functional theory (TD-DFT) calculations (Methods). The TD-DFT revealed that photoexcited electrons predominantly originate from V and Sb orbitals, as shown in density of occupied states (Supplementary Fig. 6b). This photoexcitation disturbs the local electrostatic potential experienced by Cs atoms to promote site-dependent displacements (Supplementary Movie 1). Accordingly, this photoinduced CDW breathing motion reshapes the potential energy to cause inverted displacement of one Cs ion, resulting in a three-to-one vibration (Supplementary Fig. 6c). This inversion of the Cs-ion displacement was also corroborated by potential energy surface calculations, indicating that the system reaches a lower energy state with the Cs ions at the centre of TrH (or SoD) moving toward (out of) the V superstructure (Fig. 2e). The calculation confirmed an energy gain of 6 meV by displacing the Cs ions toward the TrH centre by 0.1 Å compared to the original position (Fig. 2e). In the native L_2^- phonon mode, for the paired Cs ions, one ion was situated at the centre of the SoD (or TrH), whereas the other was not (Fig. 2d). Therefore, the native L_2^- phonon mode with two-up and two-down vibrations was incompatible with the lower energy configuration, thus being frustrated in the CDW phase. With a significant perturbation of the potential energy landscape by redistributing electronic states in the V and Sb orbitals through fs-IR laser excitation, the CDW was transiently restructured. The phonon frustration became alleviated by inverting the movement of one Cs ion to align with the lower total energy configuration of the CDW phase. This resulted in asymmetric three-up (down) and one-down (up) vibrations, consistent with the observation of the oscillatory intensity of the 2 × 2 × 2 CDW reflection (Fig. 2d).

To comprehend the impact of photoexcited electrons on frustrated phonons and CDW instability systematically, we explored the fluence dependence of fs-IR pump laser (Fig. 3). A more pronounced reduction in peak intensities was consistently observed owing to increased CDW melting with higher laser fluence (Fig. 3a). The response times for melting and subsequent short recovery appeared relatively unaffected by variations in laser fluence ranging from 0.05 to 2.5 mJ cm^{-2} (Fig. 3c, d). The melting time remained approximately 100 fs, displaying minimal dependence on laser fluence (Fig. 3c). This timescale is similarly noted for previously reported dynamics of nesting-mediated CDW systems[17,23,24]. Following this melting, there was a prompt intensity recovery, yet it failed to fully return to the intact state with the reopening of the CDW gap. This rapid recovery occurred at ~300 fs, consistent with both the 2 × 2 × 1 and 2 × 2 × 2 CDWs (Fig. 3d).

The fluence-dependent intensity of the 2 × 2 × 2 CDW exhibited intriguing characteristics warranting further investigation. Following the initial reduction upon melting, the intensity rebounded to its maximum value, showing a discernible dependence on laser fluence (Fig. 3a and b). For laser fluences exceeding approximately 0.5 mJ cm^{-2}, the intensity surpassed the intact state, denoted as 'underdamped CDW'. This transient CDW underdamping was similarly observed in other layered transition metal compounds exhibiting SoD CDW[37,38]. Subsequent to underdamping at around 400 fs, the intensity oscillated around a mean value lower than the intact state, without full recovery, persisting in a metastable state for several nanoseconds[15,16,39]. The intensity reduction in this metastable state increased with IR laser fluence until reaching approximately 1.4 mJ cm^{-2}, with a fluence dependence akin to that of the underdamped CDW intensity (Fig. 3b). Overall, the oscillation frequency of the modified coherent phonon remained largely unaffected by laser fluence, exhibiting only weak softening (1.5%) (Supplementary Note 8)[5,9,17].

We present a visual representation summarizing the overall photoinduced melting and metastable configuration of the 2 × 2 × 2 CDW (Fig. 4). The harmonic potential of the ions is schematically depicted for the CDW amplitude or mean ionic displacement (A). The potential energy of the intact 2 × 2 × 2 CDW exhibited a ground state with an initial CDW amplitude of A_0 (Fig. 4a)[40]. Fs-IR laser pumping shifted the potential energy surface (PES) to the ground state without a CDW (A = 0), indicating photoinduced gap closing (t ~ 0). With this transiently formed PES, the CDW melted to reach the ground state ($\omega t \sim \pi/2$)[41]. While adapting to this new PES, CDW underdamping occurred at $\omega t \sim \pi$ with the displacement, A_{UD}, further shifting the PES to a metastable ground state at A_{MS}. The new CDW then oscillated around the metastable ground state with an amplitude A_{MS} smaller than A_0, as observed experimentally[15,16,39]. Corresponding atomic configurations are depicted (Fig. 4b). The intact CDW, characterised by two-up and two-down displacements of Cs ions relative to the V-dimerised CDW, demonstrated frustration. Upon femtosecond modification of the electron distribution by fs-IR photoexcitation, the symmetric (two-up and two-down) phonon mode, previously frustrated, was relieved, inducing three-up (down) and one-down (up) vibrations compatible with the potential energy surface.

Discussion

In summary, we investigated the ultrafast dynamics of CDWs in the excited PES of CsV_3Sb_5 by transiently redistributing electrons near the Fermi levels using an fs-IR laser pulse. Through fs-IR photoexcitation, we induced a metastable CDW phase with a localised phonon mode, relieving the energetically frustrated two-up and two-down vibrations of Cs ions in the CDW state. This phonon mode, characterised by symmetric out-of-plane displacements of alkali ions, leads to energy loss directly coupled with the dimerization of V ions within the Kagome net, resulting in phonon frustration in the CDW phase. Restructuring the CDW using fs-IR laser photoexcitation relieves it by inducing a frustration-relieved localised phonon mode in a metastable CDW state. Our study unveiled the intricate coupling of phonons in this strongly correlated electronic system with exotic CDW phases by directly observing the modified asymmetric coherent phonons formed in a transiently disturbed potential energy configuration. It provides a concrete understanding on the mysterious roles of phonons in Kagome metals, emphasizing the crucial role of alkali ions in controlling CDW ordering[10–14]. While the phonon mode involving alkali ions' vertical motion emerges in the CDW state, noted with negative frequency in the phonon energy calculation[15], we found that this phonon mode becomes unstable in the CDW superstructure. The fs-IR photoexcitation mitigates this frustrated phonon to alter the vibration as three-up (down) and one-down (up) type, more compatible with the CDW structures. We also note that this frustration may defer immediate involvement of the L_2^- phonon to induce the CDW, explaining the absence of phonon softening in this system[5,9].

We expect this frustrated phonon dynamics is rather widespread in emerging materials. Whilst no explicit relation of the observed frustrated phonon dynamics to the superconducting transition is drawn in this study, presence of a phonon mode becoming inactive, in layered high-T_C superconductors and other layered materials, is discovered from theoretical investigations, which alludes the impact of phonon frustration in keeping the systems in the superconducting state[42]. This phonon frustration observed in this Kagome net can be direct evidence. This discovery suggests prompt investigation of similar dynamics in other correlated electronic systems and further shares common ground with understanding the energetics behind exotic charge ordering in layered high-T_C superconductors and other two-dimensional dichalcogenide materials[43–47].

Methods

Single crystal growth

Single-crystals of CsV_3Sb_5 were grown using typical self-flux methods[11,12]. Owing to the highly reactive nature of elemental Cs, the subsequent preparation of CsV_3Sb_5 was conducted inside an argon-filled glove box. Cs liquid (99.98% Alfa Aesar), acid-etched vanadium granules (99.7% Alfa Aesar), and Sb shots (99.99% Alfa Aesar) were placed in alumina crucibles with frit discs, then sealed in Ar-gas purged evacuated quartz tubes. The ampule was heated to 1000 °C for 24 h, then slowly cooled to 600 °C at a cooling rate of 5–3 °C/h. The ampule was then centrifuged to remove the flux, with any remaining flux removed via mechanical cleavage.

Time-resolved X-ray scattering experiments

Time-resolved X-ray scattering (tr-XRS) experiments were conducted at the resonant soft X-ray scattering end station of the PAL-XFEL[48]. A single-crystal specimen of CsV_3Sb_5, with its surface normal parallel to the *c*-axis, was mounted on the cold finger of a liquid helium cryostat (base temperature ~ 20 K). The diffractometer was aligned to have a horizon scattering plane with the sample *ac* plane and π-polarised incoming X-rays. X-ray pulses had a full width at half maximum pulse duration of approximately 80 fs and a repetition rate of 60 Hz. Incident X-ray photon energies were chosen to target the CDW superstructure reflections: 1240 eV for the 2 × 2 × 2 CDW at (0.5 0 1.5) reflection and 980 eV for the 2 × 2 × 1 CDW at (0.5 0 1). IR photoexcitation of the specimen was induced using a femtosecond Ti:sapphire laser system (wavelength of 800 nm and pulse duration of 50 fs root-mean-square value). The mechanical delay stage controlled the time delay between the pump and probe pulses. The focused X-ray spot size at the sample position was 100 (H) × 200 (V) μm^2, safely within the fs-IR laser footprint of 500 (H) × 500 (V) μm^2. Each single-shot X-ray scattering signal was collected using an avalanche photodiode equipped with a high-speed digitiser. For all data collection processes, data were acquired at 30 Hz by interleaving pulses for data without laser pulses to ensure the full recovery of the specimen.

X-ray scattering measurement with temperature dependence

The CDW order parameters were determined from the integrated intensity of the CDW reflections through X-ray scattering experiments conducted at the synchrotron 6 A beamline of the PLS. Crystals were cryo-cooled using a liquid helium cryostat. The photon energy was fixed at 1580 eV, covering the 2 × 2 × 2 (0.5 0 1.5) and 2 × 2 × 1 (0.5 0 2) reflections.

Time-dependent density functional calculation

To investigate the total energy, optimised lattice parameters, and electronic structure in the ground state of CsV_3Sb_5 through first-principles calculations, density functional theory calculations were

performed using the Quantum Espresso package[49]. The optimised lattice parameters for the $2 \times 2 \times 2$ trigonal CsV_3Sb_5 system were $a = 10.88$ Å and $c = 18.66$ Å. Kohn-Sham wave functions were illuminated by a plane wave with an energy cut-off of 60 Ry. The Perdew (Burke) Ernzerhof generalised gradient approximation functional was employed to describe electron-electron exchange and correlations[50]. Core electrons and their effects on valence electrons were addressed using norm-conserving pseudopotentials. The Brillouin zone was sampled using a Monkhorst pack with a $3 \times 3 \times 2$ mesh. Ionic structure relaxation was achieved by optimising positions with the force criteria of 1.0×10^{-5} eV Å^{-1}.

To investigate light-induced dynamics using a first-principles approach, we employed Ehrenfest dynamics with real-time TD-DFT[51]. For time propagation, we utilised a Crank-Nicolson-type time-evolution operator with a time step of 4.8 attoseconds. The optimised Alternative SoD and TrH superstructures[10,21] served as the initial geometries for the TD-DFT calculations. An oscillating electric field of gaussian-packet type (E(t)) was applied to the system through the vector potential term, with $E(t) = dA/dt$ with $A(t) = A_0 e^{-0.5[(t-t_0)/\sigma]^2} \sin \omega t$. The laser parameters in the simulation were set to match experimental conditions: $\hbar\omega = 1.54$ eV and $\sigma = 80$ fs, with a laser power density of 3.6×10^{10} W cm^{-2} and 25% reduced power of 2.7×10^{10} W cm^{-2}. Both power densities produced the same results qualitatively supporting that the interpretation is generally valid without specific laser fluence dependence. The detailed calculation settings mirrored those of the DFT calculations, except for the Brillouin zone sampling (1×1×1).

Data availability

Source data related to the dynamics of CDW orders presented in this paper are provided. The atomic coordinates of the initial and final configurations from the Ehrenfest dynamics simulations have been deposited in figshare under the https://doi.org/10.6084/m9.figshare.28838315. Additional data supporting the findings of this study are available from the corresponding authors upon request. Source data are provided with this paper.

Code availability

The real-time TDDFT code used in this study is available from the corresponding authors upon request.

References

1. Zhao, H. et al. Cascade of correlated electron states in the kagome superconductor CsV_3Sb_5. *Nature* **599**, 216–221 (2021).
2. Nie, L. et al. Charge-density-wave-driven electronic nematicity in a kagome superconductor. *Nature* **604**, 59–64 (2022).
3. Jiang, Y.-X. et al. Unconventional chiral charge order in kagome superconductor KV_3Sb_5. *Nat. Mater.* **20**, 1353–1357 (2021).
4. Kang, M. et al. Twofold van Hove singularity and origin of charge order in topological kagome superconductor CsV_3Sb_5. *Nat. Phys.* **18**, 301–308 (2022).
5. Li, H. et al. Observation of Unconventional Charge Density Wave without Acoustic Phonon Anomaly in Kagome Superconductors AV_3Sb_5 (A = Rb, Cs). *Phys. Rev. X* **11**, 031050 (2021).
6. Grüner, G. *Density waves in solids* (Westview Press, 2009).
7. Tan, H., Liu, Y., Wang, Z. & Yan, B. Charge Density Waves and Electronic Properties of Superconducting Kagome Metals. *Phys. Rev. Lett.* **127**, 046401 (2021).
8. Ortiz, B. R. et al. Fermi Surface Mapping and the Nature of Charge-Density-Wave Order in the Kagome Superconductor CsV_3Sb_5. *Phys. Rev. X* **11**, 041030 (2021).
9. Subires, D. et al. Order-disorder charge density wave instability in the kagome metal $(Cs,Rb)V_3Sb_5$. *Nat. Commun.* **14**, 1015 (2023).
10. Kang, M. et al. Charge order landscape and competition with superconductivity in kagome metals. *Nat. Mater.* **22**, 186–193 (2023).
11. Ortiz, B. R. et al. New kagome prototype materials: discovery of KV_3Sb_5, RbV_3Sb_5, and CsV_3Sb_5. *Phys. Rev. Mater.* **3**, 094407 (2019).
12. Ortiz, B. R. et al. CsV_3Sb_5: A $\mathbb{Z}_2$ Topological Kagome Metal with a Superconducting Ground State. *Phys. Rev. Lett.* **125**, 247002 (2020).
13. Ortiz, B. R. et al. Superconductivity in the $\mathbb{Z}_2$ kagome metal KV_3Sb_5. *Phys. Rev. Mater.* **5**, 034801 (2021).
14. Yin, Q. et al. Superconductivity and Normal-State Properties of Kagome Metal RbV_3Sb_5 Single Crystals. *Chin. Phys. Lett.* **38**, 037403 (2021).
15. Ratcliff, N., Hallett, L., Ortiz, B. R., Wilson, S. D. & Harter, J. W. Coherent phonon spectroscopy and interlayer modulation of charge density wave order in the kagome metal CsV_3Sb_5. *Phys. Rev. Mater.* **5**, L111801 (2021).
16. Yu, J. et al. All-optical manipulation of charge density waves in kagome metal CsV_3Sb_5. *Phys. Rev. B* **107**, 174303 (2023).
17. Azoury, D. et al. Direct observation of the collective modes of the charge density wave in the kagome metal CsV_3Sb_5. *Proc. Natl Acad. Sci. USA* **120**, e2308588120 (2023).
18. Han, S. et al. Orbital-hybridization-driven charge density wave transition in CsV_3Sb_5 kagome superconductor. *Adv. Mater.* **35**, 2209010 (2023).
19. Li, H. et al. Discovery of conjoined charge density waves in the kagome superconductor CsV_3Sb_5. *Nat. Commun.* **13**, 6348 (2022).
20. Christensen, M. H., Birol, T., Andersen, B. M. & Fernandes, R. M. Theory of the charge density wave in AV_3Sb_5 kagome metals. *Phys. Rev. B* **104**, 214513 (2021).
21. Hu, Y. et al. Coexistence of trihexagonal and star-of-David pattern in the charge density wave of the kagome superconductor AV_3Sb_5. *Phys. Rev. B* **106**, L241106 (2022).
22. Song, C. et al. Charge-density-wave orderings in $LaAgSb_2$: An x-ray scattering study. *Phys. Rev. B* **68**, 035113 (2003).
23. Rohwer, T. et al. Collapse of long-range charge order tracked by time-resolved photoemission at high momenta. *Nature* **471**, 490–493 (2011).
24. Hellmann, S. et al. Time-domain classification of charge-density-wave insulators. *Nat. Commun.* **3**, 1069 (2012).
25. Allen, P. B. Theory of thermal relaxation of electrons in metals. *Phys. Rev. Lett.* **59**, 1460–1463 (1987).
26. Zeiger, H. J. et al. Theory for displacive excitation of coherent phonons. *Phys. Rev. B* **45**, 768–778 (1992).
27. Garrett, G. A., Albrecht, T. F., Whitaker, J. F. & Merlin, R. Coherent THz Phonons Driven by Light Pulses and the Sb Problem: What is the Mechanism?. *Phys. Rev. Lett.* **77**, 3661–3664 (1996).
28. Sokolowski-Tinten, K. et al. Femtosecond X-ray measurement of coherent lattice vibrations near the Lindemann stability limit. *Nature* **422**, 287–289 (2003).
29. Fritz, D. M. et al. Ultrafast Bond Softening in Bismuth: Mapping a Solid's Interatomic Potential with X-rays. *Science* **315**, 633–636 (2007).
30. Huber, T. et al. Coherent Structural Dynamics of a Prototypical Charge-Density-Wave-to-Metal Transition. *Phys. Rev. Lett.* **113**, 026401 (2014).
31. Cheng, Y. et al. Ultrafast formation of topological defects in a two-dimensional charge density wave. *Nat. Phys.* **20**, 54–60 (2024).
32. Vinograd, I. et al. Locally commensurate charge-density wave with three-unit-cell periodicity in $YBa_2Cu_3O_y$. *Nat. Commun.* **12**, 3274 (2021).
33. Kim, H. J. et al. Local Atomic Structure and Discommensurations in the Charge Density Wave of $CeTe_3$. *Phys. Rev. Lett.* **96**, 226401 (2006).
34. Trigo, M. et al. Fourier-transform inelastic X-ray scattering from time- and momentum-dependent phonon–phonon correlations. *Nat. Phys.* **9**, 790–794 (2013).
35. Wall, S. et al. Ultrafast disordering of vanadium dimers in photo-excited VO_2. *Science* **362**, 572–576 (2018).

36. Hirota, K., Hill, J. P., Shapiro, S. M., Shirane, G. & Fujii, Y. Neutron- and x-ray-scattering study of the two length scales in the critical fluctuations of SrTiO3. *Phys. Rev. B* **52**, 13195–13205 (1995).
37. Zhang, Y. et al. Creation of a novel inverted charge density wave state. *Struct. Dyn.* **9**, 014501 (2022).
38. Zhang, J. et al. Photoexcitation Induced Quantum Dynamics of Charge Density Wave and Emergence of a Collective Mode in 1*T*-TaS2. *Nano Lett.* **19**, 6027–6034 (2019).
39. Mihaly, L., Lee, K.-B. & Stephens, P. W. X-ray diffraction study of the metastable charge-density-wave state of $K_{0.3}MoO_3$. *Phys. Rev. B* **36**, 1793–1795 (1987).
40. Littlewood, P. B. & Varma, C. M. Amplitude collective modes in superconductors and their coupling to charge-density waves. *Phys. Rev. B* **26**, 4883–4893 (1982).
41. Singer, A. et al. Photoinduced Enhancement of the Charge Density Wave Amplitude. *Phys. Rev. Lett.* **117**, 056401 (2016).
42. Lee, S. et al. Thermal decoupling in high-Tc cuprate superconductors. Preprint at *arXiv* https://doi.org/10.48550/arXiv.2303.11600 (2023).
43. Cao, Y. et al. Unconventional superconductivity in magic-angle graphene superlattices. *Nature* **556**, 43–50 (2018).
44. Si, Q., Yu, R. & Abrahams, E. High-temperature superconductivity in iron pnictides and chalcogenides. *Nat. Rev. Mater.* **1**, 16017 (2016).
45. Kogar, A. et al. Light-induced charge density wave in $LaTe_3$. *Nat. Phys.* **16**, 159–163 (2020).
46. Disa, A. S., Nova, T. F. & Cavalleri, A. Engineering crystal structures with light. *Nat. Phys.* **17**, 1087–1092 (2021).
47. Fausti, D. et al. Light-Induced Superconductivity in a Stripe-Ordered Cuprate. *Science* **331**, 189–191 (2011).
48. Jang, H. et al. Time-resolved resonant elastic soft x-ray scattering at Pohang Accelerator Laboratory X-ray Free Electron Laser. *Rev. Sci. Instrum.* **91**, 083904 (2020).
49. Giannozzi, P. et al. QUANTUM ESPRESSO: A modular and open-source software project for quantum simulations of materials. *J. Phys. Condens. Matter* **21**, 395502 (2009).
50. Perdew, J. P., Burke, K. & Ernzerhof, M. Generalized Gradient Approximation Made Simple. *Phys. Rev. Lett.* **77**, 3865–3868 (1996).
51. Shin, D., Lee, G., Miyamoto, Y. & Park, N. Real-Time Propagation via Time-Dependent Density Functional Theory Plus the Hubbard U Potential for Electron–Atom Coupled Dynamics Involving Charge Transfer. *J. Chem. Theory Comput.* **12**, 201–208 (2016).

Acknowledgements

C.S. appreciates Prof. K.-W. Kim for insightful discussion on the coherent phonon dynamics and Prof. G.-D. Lee on the abnormal lattice vibrations of interlayer alkali metal ions. X-ray scattering experiments at PAL are approved by the Korean Synchrotron Users Association (KOSUA). This work was supported by the National Research Foundations (NRF) of Korea (grant Nos. 2020K1A3A7A09080405, 2022M3H4A1A04074153, RS-2024-00346711, RS-2024-00333664 and RS-2023-00218180). The computational work was supported by the National Supercomputing Center with supercomputing resources including technical support (KSC-2024-CRE-0124).

Author contributions

C.S. supervised the project. C.S. and J.-H.P. conceived the project. S.-P.H., H.L., E.P., S.Y.L., J.H., B.L., H.J. and W.-S.N. performed the X-ray scattering experiments. C.W. synthesized the crystals. S.-P.H., H.L. and C.S. analyzed the data. H.C. maintained the fs-IR laser. S.Y.P. worked on the DAQ system. H.K. and D.S. performed the first-principle calculations. S.-P.H. and C.S. wrote the manuscript with input from all authors.

Competing interests

The authors declare no competing interests.

Additional information

Supplementary information The online version contains supplementary material available at https://doi.org/10.1038/s41467-025-60219-0.

Correspondence and requests for materials should be addressed to Dongbin Shin or Changyong Song.

Peer review information *Nature Communications* thanks the anonymous reviewer(s) for their contribution to the peer review of this work. A peer review file is available.